Langmuir
Article
pubs.acs.org/Langmuir

Evaluating Glutamate and Aspartate Binding Mechanisms to Rutile (α-TiO_2) via ATR-FTIR Spectroscopy and Quantum Chemical Calculations

Sanjai J. Parikh,*[,†] James D. Kubicki,[⊥] Caroline M. Jonsson,[‡,§] Christopher L. Jonsson,[‡,§] Robert M. Hazen,[‡] Dimitri A. Sverjensky,[‡,§] and Donald L. Sparks[∥]

[†]*Department of Land, Air and Water Resources, University of California, Davis, California 95616, United States,* [‡]*Geophysical Laboratory, Carnegie Institution of Washington, 5251 Broad Branch Road, Washington, D.C. 20008, United States,* [§]*Department of Earth and Planetary Sciences, Johns Hopkins University, Baltimore, Maryland 21218, United States,* [∥]*Department of Plant and Soil Sciences and Center for Critical Zone Research, The University of Delaware, Newark, Delaware 19716, United States, and* [⊥]*Department of Geosciences and The Earth & Environmental Systems Institute, The Pennsylvania State University, University Park, Pennsylvania 16802, United States*

Received September 23, 2010. Revised Manuscript Received December 20, 2010

Attenuated total reflectance (ATR) Fourier transform infrared (FTIR) spectroscopy and quantum chemical calculations were used to elucidate the influence of solution chemistry (pH, amino acid concentration) on the binding mechanisms of glutamic and aspartic acid to rutile (α-TiO_2). The amino acids, glutamate and aspartate, contain carboxyl and amine groups whose dissociation over a pH range results in changes of molecular charge and reactivity, including reactions with mineral surfaces. At pH 3, a decrease of IR bands corresponding to protonated carboxyl groups is observed upon reaction with TiO_2 and indicates involvement of distal carboxyl groups during sorption. In addition, decreased IR bands arising from carboxyl bonds at 1400 cm^{-1}, concomitant to shifts to higher wavenumbers for ν_{as}(γ-COO^-) and ν_{as}(α-COO^-) (particularly at low glutamate concentrations), are indicative of inner-sphere coordination of both carboxyl groups and therefore suggest a "lying down" surface species. IR spectra of aspartate reacted with rutile are similar to those of solution-phase samples, without peak shifts indicative of covalent bonding, and outer-sphere coordination is predicted. Quantum chemical calculations were carried out to assist in elucidating molecular mechanisms for glutamate binding to rutile and are in reasonable agreement with experimental data. The combined use of ATR-FTIR data and quantum calculations suggests three potential surface configurations, which include (1) bridging-bidentate where glutamate is "lying down" and binding occurs through inner-sphere coordination of both α- and γ-carboxyl groups; (2) chelating-monodentate in which glutamate binds through inner-sphere coordination with the γ-carboxyl group in a "standing up" configuration (with or without protonation of the α-carboxyl); and (3) another bridging-bidentate configuration where glutamate is binding to rutile via inner-sphere coordination of the α-carboxyl group and outer-sphere coordination with the γ-carboxyl ("lying down").

1. Introduction

Interactions between amino acids and mineral surfaces are of fundamental importance for understanding bacterial adhesion, biomolecule transport, mineral dissolution, elemental cycling, long-term functionality of implanted medical devices, and, perhaps, the origin of life. Due to the ubiquitous occurrence of amino acids in soil, water, and the human body, their binding to a wide range of mineral surfaces is commonplace. Amino acids have a propensity for self-organization on surfaces and therefore possess the ability to functionalize solid surfaces.[1−3] If amino acids bind to mineral surfaces in an organized manner, they may serve as templates for additional molecules to bind in predictable arrangements.

While amino acid binding to hydroxylated surfaces is of great importance to a number of disciplines,[4] the current understanding of how amino acids attach to mineral surfaces remains inadequate. To address the need for this information, a number of recent studies have been published to examine the interactions of L-glutamic acid (glutamate) and L-aspartic acid (aspartate) with TiO_2 surfaces.[1,2,5−8] Attenuated total reflectance (ATR) Fourier transform infrared (FTIR) spectroscopy was used to examine the binding of glutamate and aspartate to amorphous TiO_2.[1] Results from this study reveal one major adsorbed aspartate species and several adsorbed species of glutamate to the TiO_2. A follow up study utilized the glutamate IR data and predicted glutamate binding via carboxyl groups through at least three surface species: (1) bridging-bidentate with four points of attachment; (2) chelating-monodentate with three points of attachment; and (3) chelating with two points of attachment through the γ-carboxyl group.[7]

Sum frequency generation vibrational spectroscopy of amino acid interactions with TiO_2 revealed that glutamate and aspartate form ordered and fairly homogeneous adsorbate layers on TiO_2.[2,8] Additionally, it was observed that amino acids without carboxyl side chains (i.e., glutamine, phenylalanine) have low

*To whom correspondence should be addressed. E-mail: sjparikh@ucdavis.edu.

(1) Roddick-Lanzilotta, A. D.; McQuillan, A. J. *J. Colloid Interface Sci.* **2000**, *227*, 48–54.
(2) Pászti, Z.; Guczi, L. *Vib. Spectrosc.* **2009**, *50*, 48–56.
(3) Barlow, S. M.; Raval, R. *Surf. Sci. Rep.* **2003**, *50*, 201–341.
(4) Lambert, J. F. *Origins Life Evol. Biospheres* **2008**, *38*, 211–242.
(5) Jonsson, C. M.; Jonsson, C. L.; Estrada, C.; Sverjensky, D. A.; Cleaves, H. J.; Hazen, R. M. *Geochim. Cosmochim. Acta* **2010**, *74*, 2356–2367.
(6) Jonsson, C. M.; Jonsson, C. L.; Sverjensky, D. A.; Cleaves, H. J.; Hazen, R. M. *Langmuir* **2009**, *25*, 12127–12135.
(7) Sverjensky, D. A.; Jonsson, C. M.; Jonsson, C. L.; Cleaves, H. J.; Hazen, R. M. *Environ. Sci. Technol.* **2008**, *42*, 6034–6039.
(8) Pászti, Z.; Keszthelyi, T.; Hakkel, O.; Guczi, L. *J. Physics: Condens. Matter* **2008**, 20.

affinity for TiO_2 surfaces and that aspartate binds through both carboxyl groups, one monodentate and one stabilized via hydrogen bonding.[2] Similar results for glutamate were observed but not discussed in detail. A slightly different bridging surface species of aspartate to TiO_2 has also been proposed from ATR-FTIR spectroscopy results with aspartate coordinated via bidentate complexes with carboxyl groups to two Ti atoms.[1] The use of quantum chemical calculations can be of great benefit for interpreting vibrational spectroscopy to aid in elucidation of molecular binding mechanisms;[9−12] however, to our knowledge, only two previous papers have been published using quantum mechanics to examine amino acid (glycine and proline;[13] glycine, methionine, serine, cysteine[14]) interactions with TiO_2. The results of these studies indicate that sorption for these monocarboxylic amino acids is mediated by carboxyl groups forming inner-sphere complexes at the mineral surface. These studies also suggest additional stabilization of the surface complex via H-bonding between amino groups and the protonated surface.

Sorption experiments examining glutamate and aspartate binding to rutile (α-TiO_2) reveal strong binding from pH 3 to 5 with decreased sorption observed with increasing ionic strength.[5,6] Surface complexation models of these interactions indicate the presence of at least two glutamate−rutile complexes, which are influenced by pH and glutamate concentration: binding through both carboxyl groups in a bridging-bidentate configuration ("lying down"), a chelating species binding through the γ-carboxyl group ("standing up"), or via outer-sphere complexation with the γ-carboxyl group.[6] The four points of attachment hypothesized for the bridging-bidentate species involved four adjacent surface titanium sites. These could conceivably occur on several crystal planes of the ideal rutile structure, including the (110) surface which is typically the most abundant.[6] However, the two points of attachment for the chelating species were suggested to belong to only one titanium (e.g., $>Ti(OH)_2$-type sites). Such sites are not found on the ideal (110) plane but are instead found on common pyramidal forms such as those containing the (101) or (111) planes.[15] Modeling for aspartate sorption to rutile predicted similar, and analogous, surface species.[5]

The current study uses similar experimental conditions and in situ ATR-FTIR spectroscopy to probe the binding mechanisms of glutamate and aspartate to rutile, a crystalline form of TiO_2. In addition to ATR-FTIR data, quantum chemical calculations have been carried out to model the interactions of glutamate with rutile and to help elucidate mechanisms of sorption. The primary objective of this paper is to improve the current understanding of the mechanisms of attachment for glutamate and aspartate to rutile under varying environmental conditions. This research builds on our fundamental knowledge of sorption mechanisms and surface coordination of carboxylated amino acids on oxyhydroxide minerals. This basic understanding of initial binding is needed to evaluate subsequent geochemical processes, ranging from organic contaminant fate and transport to understanding the formation of organic templates in early earth environments.

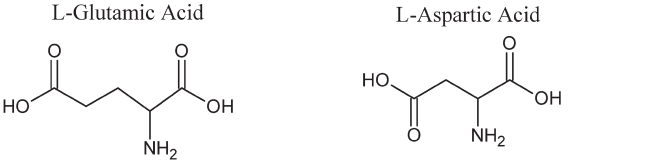

Figure 1. Chemical structures and properties of glutamate and aspartate.

2. Experimental Procedures

2.1. Materials. All solutions were prepared in polypropylene vials using Barnstead Nanopure (BNP; 18.2 MΩ·cm) water with pH adjustment via 100 mmol kg^{-1} NaOH/HCl. Stock 40 mmol kg^{-1} solutions of L-glutamic acid (Acros Organics, 99%) and L-aspartic Acid (Arcos Organics, 98+%) were prepared in 100 mmol kg^{-1} NaCl (Figure 1). The pH of 40 mmol kg^{-1} stocks were adjusted to 1.5, 3.3, 4.1, 5, 5.8, and 7.1 for glutamate and 3.3 and 6.2 for aspartate for use as unreacted aqueous phase standards. For experiments with rutile, stock solutions of glutamate and aspartate were diluted with 100 mmol kg^{-1} NaCl to 4.4, 1, and 0.1 mmol kg^{-1} (glutamate or aspartate) and pH adjusted (pH ∼3 and∼ 6) for individual experiments.

Rutile powder (α-TiO_2, pH_{PZC} = 5.4) was obtained from Oak Ridge National Laboratory (courtesy of J. Rosenqvist, D. Wesolowski, and M. Machesky). At Oak Ridge National Laboratory, rutile powder from Tioxide Specialties Ltd. (Cleveland, U.K.) was pretreated using published procedures.[16] A description of the cleaning processes is given in Jonsson et al.[6] A specific surface area of 18.1 ± 0.1 m^2 g^{-1} was determined using the Brunauer−Emmett−Teller (BET) N_2 adsorption method.[17] Upon receipt, X-ray powder diffraction (XRD) was conducted to confirm that the resulting particles were rutile, and scanning electron microscopy (SEM) showed that the particles are needle shaped, approximately 50−100 nm wide and 400−500 nm long.[6] The predominant growth face is (110). The crystal-termination faces appear to be (101) and (111). The extent to which these faces may be present as steps on the (110) face is not known but is assumed in the present study to be significant because these planes (and not the 110) have the appropriate surface functional groups for the chelating surface species hypothesized previously based on surface complexation modeling of adsorption data.[6] Rutile suspensions of 10 g kg^{-1} were adjusted to pH 4.3 and equilibrated overnight prior to use in experiments.

2.2. Rutile Coatings for ATR-FTIR Experiments. The use of coatings on ATR internal reflection elements (IRE) is a well established technique to examine binding mechanisms of various organic and inorganic samples to metal oxide surfaces.[18−21] Because sorption leads to an increased accumulation of compounds at the IRE−water interface, this technique permits examination of very low concentrations of compounds, assuming sorption to the IRE coating. In the current study, the ZnSe IRE was coated with rutile by depositing 1 mL of 10 g kg^{-1} (pH 4.3) rutile onto the IRE and drying in air overnight at 37 °C. A pH of 4.3 was used to allow favorable electrostatic interaction for rutile binding to ZnSe; the point of zero charge of rutile is 5.4 and the isoelectric point of ZnSe is <4.[22] After drying, the rutile coating

(9) Kubicki, J. D.; Kwon, K. D.; Paul, K. W.; Sparks, D. L. *Eur. J. Soil Sci.* **2007**, *58*, 932–944.
(10) Mendive, C. B.; Bredow, T.; Blesa, M. A.; Bahnemann, D. W. *Phys. Chem. Chem. Phys.* **2006**, *8*, 3232–3247.
(11) Ferrari, A. M.; Huber, S.; Knozinger, H.; Neyman, K. M.; Rosch, N. *J. Phys. Chem. B* **1998**, *102*, 4548–4555.
(12) Omoike, A.; Chorover, J.; Kwon, K. D.; Kubicki, J. D. *Langmuir* **2004**, *20*, 11108–11114.
(13) Tonner, R. *ChemPhysChem* **2010**, *11*, 1053–1061.
(14) Langel, W.; Menken, L. *Surf. Sci.* **2003**, *538*, 1–9.
(15) Koretsky, C. M.; Sverjensky, D. A.; Sahai, N. *Am. J. Sci.* **1998**, *298*, 349–438.
(16) Machesky, M. L.; Wesolowski, D. J.; Palmer, D. A.; Ichiro-Hayashi, K. *J. Colloid Interface Sci.* **1998**, *200*, 298–309.
(17) Brunauer, S.; Emmett, P. H.; Teller, E. *J. Am. Chemi. Soc.* **1938**, *60*, 309–319.
(18) Hug, S. J. *J. Colloid Interface Sci.* **1997**, *188*, 415–422.
(19) Parikh, S. J.; Chorover, J. *Langmuir* **2006**, *22*, 8492–8500.
(20) Lefevre, G. *Adv. Colloid Interface Sci.* **2004**, *107*, 109–123.
(21) Hug, S. J.; Sulzberger, B. *Langmuir* **1994**, *10*, 3587–3597.
(22) Tickanen, L. D.; Tejedor-Tejedor, M. I.; Anderson, M. A. *Langmuir* **1997**, *13*, 4829–4836.

was washed with a gentle stream of BNP water to remove any loosely adhered particles.

2.3. ATR-FTIR Spectroscopy. FTIR spectra for glutamate and aspartate were collected with a Thermo Nicolet Nexus 670 spectrometer using a horizontal 10-bounce accessory (PIKE Technologies HATR) with a ZnSe IRE at ambient temperature (23 ± 1 °C). Due to the low pH of the aqueous glutamate standard at pH 1.5, which would begin to dissolve the ZnSe IRE, the FTIR spectrum for pH 1.5 glutamate was collected using a single-bounce diamond ATR IRE (SmartOrbit, Thermo). Spectra were collected using standard collection techniques via the Omnic 7.0 (Thermo) software package, with 128 scans at 4 cm^{-1} and a MCT/A detector. Spectra of aqueous phase glutamate and aspartate standards were collected with a ZnSe background followed by subtraction of a 100 mmol kg^{-1} NaCl spectrum at the appropriate pH. In these experiments, concentrations of aqueous glutamate and aspartate subsequent to reaction with rutile films are below detection limits and contributions of unbound amino acids not observed in IR spectra. A minimum of duplicate experiments/spectra were collected to verify reproducibility of results. The wavenumber of FTIR peaks was confirmed via second derivative analysis (Thermo, Omnic 7.0).

Experiments were conducted by depositing 1 mL of either glutamate or aspartate onto the rutile coated ZnSe IRE. FTIR spectra of glutamate or aspartate were collected after 35 min of reaction. To ensure collected spectra represented only bound amino acid, the amino acid solution was gently poured off the IRE (after 35 min of reaction) to remove unbound amino acid and 1 mL of 100 mmol kg^{-1} NaCl was deposited on the reacted rutile coating and spectra were collected. The spectra of amino acids reacted with rutile were acquired with a ZnSe background with subsequent subtraction of a spectrum of hydrated rutile coating at the appropriate pH. Selected experiments were also conducted with N_2 purged solutions and suspensions with ATR-FTIR collection under a N_2 environment to verify no interference of atmospheric CO_2 with TiO_2 films.

2.4. Quantum Chemical Calculations. *2.4.1. Model Building*. Models of aqueous glutamic acid ($C_5O_4NH_{10}$) were created in the +1, 0, and −1 charged states using the 3-D Sketcher module of Cerius[2] software,[23] and 14 H_2O molecules were added manually to H-bond to each of the polar groups of the glutamic acid. The "Clean" utility was used to create the initial guess for the structure. Cartesian coordinates were then extracted and used as inputs for Gaussian 03 energy minimizations.[24] These models of aqueous glutamic acid species were used to benchmark the computational methodology against observed vibrational spectra of glutamic acid in water.

Previous molecular modeling and surface complexation studies of protons and metals on rutile have emphasized the predominance of the (110) crystal plane and its importance in accounting for the adsorption of these species.[25−28] However, as already indicated above, the surface complexation modeling of glutamate adsorption on our rutile indicated that a chelating surface species was predicted to be the most abundant surface glutamate species at the highest surface loadings. The appropriate surface functional groups for this species are not present on the ideal rutile (110) plane but are present on the (101) and (111) planes. These planes appear to form the terminations on the crystals of our sample, and may well be present as steps on the (110) surface. Consequently, in the present study, we focused on the (101) plane.

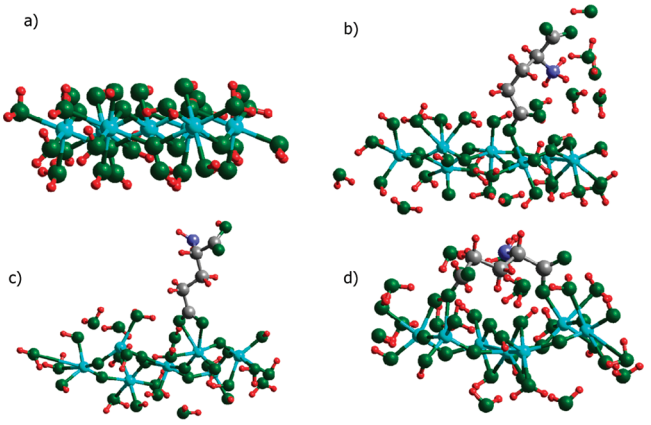

Figure 2. Model rutile surface and glutamate clusters on rutile with H_2O used for quantum chemical calculations: (a) Initial model of the rutile (α-TiO_2) (101) surface created with the software package Cerius[2] (Accelrys Inc., San Diego, CA). Ti , light blue; O, green; C, gray; N, blue; H, red. (b) Monodentate, mononuclear, configuration through γ-COO^-, (c) bidentate, mononuclear, configuration through γ-COO^-, and (d) monodentate, mononuclear, configuration through both α- and γ-COO^-. H_2O molecules H-bonding to glutamate shown in (b) and (d); "dry" case is shown in (c).

Rutile (101) surface models were created by cleaving the bulk rutile structure along the (101) direction using the Surface Model Builder module of Cerius[2].[23] A structure based on 7 Ti atoms and all the O atoms (34 O atoms total) bonded to these Ti atoms was then extracted by deleting the atoms outside of this group. H atoms were added to refill the valences of the O atoms on the edge of the cluster to create a neutrally charged cluster representing the surface (Figure 2a). Glutamate in various charged states was docked to this cluster in monodentate/bidentate mononuclear and monodentate binuclear configurations (Figure 2b−d) with the carboxyl groups replacing the original OH or OH_2 groups of the model surface cluster. In total, three aqueous-phase glutamate models and 13 glutamate configurations on the (101) surface of rutile (4 monodentate mononuclear, 6 bidentate mononuclear, 3 monodentate binuclear) were determined to lead to stable configurations and compared with experimental data. Attempts to build bidentate models (e.g., Figure 2c) through one or two carboxyl groups were unsuccessful as calculations predict that this configuration is not stable. In one instance during energy minimization, one bond of a bidentate mononuclear configuration broke and resulted in a monodentate mononuclear surface species.

2.4.2. Energy Minimization. Energy minimizations were performed within Gaussian 03 using the default criteria for forces and displacements. No symmetry or other constraints were imposed during this optimization procedure. Structural relaxations were performed in two stages. The first step included freezing the Ti atom positions in their experimental lattice positions while all other atoms were relaxed. This partial relaxation helps ensure that the final product is similar to experimental crystal surface. After this partial relaxation, a second energy minimization was performed allowing all atoms to move. Thus, the models were in local minima (as verified by frequency analyses discussed below). In the final energy-minimized structures, displacements of Ti atoms were less than 1 Å from the original crystallographic positions; thus, the cluster model of the surface retains a significant amount of the surface structure although the surface relaxation may be somewhat exaggerated compared to a real crystal surface.

(23) Accelrys. *Cerius[2] Modeling Environment*; Accelrys, Inc.: San Diego, CA, 2003.
(24) Frisch, M. J. et al. *Gaussian 03*, revision C.02; Gaussian Inc.: Wallingford, CT, 2004.
(25) Zhang, Z.; Fenter, P.; Kelly, S. D.; Catalano, J. G.; Bandura, A. V.; Kubicki, J. D.; Sofo, J. O.; Wesolowski, D. J.; Machesky, M. L.; Sturchio, N. C.; Bedzyk, M. J. *Geochim. Cosmochim. Acta* **2006**, *70*, 4039–4056.
(26) Zhang, Z.; Fenter, P.; Cheng, L.; Sturchio, N. C.; Bedzyk, M. J.; Predota, M.; Bandura, A.; Kubicki, J. D.; Lvov, S. N.; Cummings, P. T.; Chialvo, A. A.; Ridley, M. K.; Benezeth, P.; Anovitz, L.; Palmer, D. A.; Machesky, M. L.; Wesolowski, D. J. *Langmuir* **2004**, *20*, 4954–4969.
(27) Predota, M.; Zhang, Z.; Fenter, P.; Wesolowski, D. J.; Cummings, P. T. *J. Phys. Chem. B* **2004**, *108*, 12061–12072.
(28) Predota, M.; Bandura, A. V.; Cummings, P. T.; Kubicki, J. D.; Wesolowski, D. J.; Chialvo, A. A.; Machesky, M. L. *J. Phys. Chem. B* **2004**, *108*, 12049–12060.

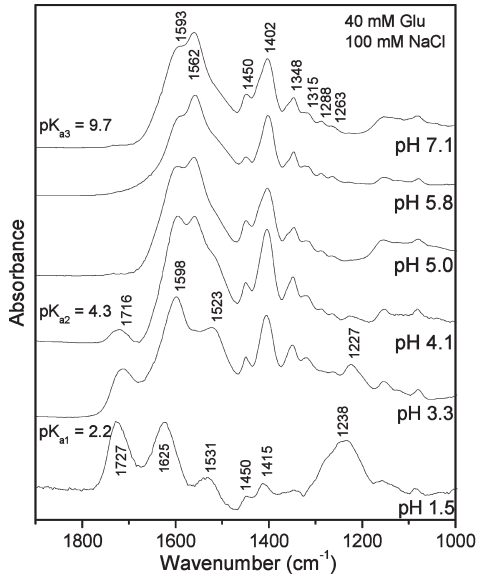

Figure 3. ATR-FTIR spectra of aqueous glutamate for a range of pH values (mM = mmol kg^{-1}).

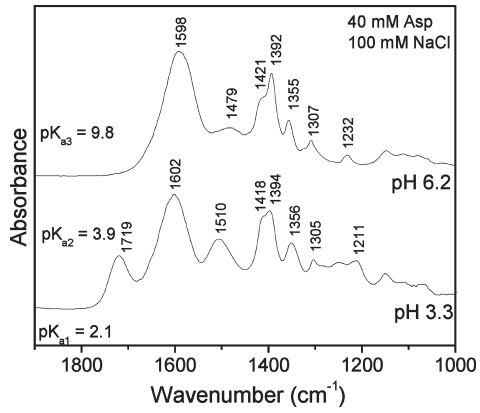

Figure 4. ATR-FTIR spectra of aqueous aspartate for a range of pH values (mM = mmol kg^{-1}).

Energy minimizations were conducted with and without H_2O molecules solvating the polar groups of the glutamic acid to test for the effects of adsorbed water vapor on the calculated vibrational frequencies. The Becke[29] three-parameter exchange functional and the Lee et al.[30] correlation functional were used along with the 6-31G(d)[31] basis set (i.e., B3LYP/6-31G(d)) to model the electron densities and obtain molecular energies.

2.4.3. Frequency Analyses. Using the energy-minimized structures, analytical frequencies were calculated (i.e., G03 analytically solves for the eigenvalue and eigenvectors of the second-derivative potential energy matrix or Hessian[32]). The infrared (IR) and Raman intensities were also calculated analytically using the methods built into the G03 program.[33,34] Model frequencies were scaled by 0.96 to account for systematic errors involving basis set limitations,[32] electron correlation approximations, and anharmonicity. Vibrational modes were visualized using the software Molden[35] to determine which frequencies were associated with motion of the carboxyl groups of the glutamic acid.

3. Results and Discussion

3.1. Aqueous Phase FTIR Spectra. The FTIR spectra of aqueous glutamate and aspartate are shown in Figures 3 and 4 (water spectra subtracted), respectively, and IR band locations are consistent with previous studies.[1,36−38] The pK_a values for carboxyl and amine groups are included in the figures, and the effect of functional group protonation on the IR spectra with decreasing pH is observed. It is important to note that, for glutamate, pK_{a1} corresponds to the α-carboxyl (close to the amine group) and the pK_{a2} corresponds to the γ-carboxyl (distal).[1] Examination of spectra as a function of pH highlights the different pK_a values for the α- and γ-carboxyl groups. The presence of peaks at different locations for α- and γ-carboxyl groups can be informative when elucidating binding mechanisms to determine participation of specific carboxyl groups. Band assignments for aqueous glutamate and aspartate at pH 3 and 6 are given in Tables 1 and 2, respectively. At high pH values, both carboxyl groups are deprotonated and separate peaks for the ν_{as}(α-COO$^-$) and ν_{as}(γ-COO$^-$) are observed. As the solution pH is decreased and the γ-carboxyl is protonated, a peak at ∼1720 cm^{-1} [ν(γ-C═O)] is detected while the ν_{as}(γ-COO$^-$) (1562 cm^{-1}) disappears and the mixed (α and γ) ν_s(COO$^-$) decreases in relative intensity. Additionally, as the pH is lowered, the amine can be detected as a peak that appears around 1515−1530 cm^{-1}. Calculations of IR frequency for aqueous glutamate at pH 3 and 6 are in general agreement with experimental data, and linear regression of observed versus calculated frequencies results in R^2 values of 0.993 (N = 8) and 0.995 (N = 5), respectively, with slopes near unity and y-intercepts approaching the origin (Table 2). Experimental peaks were matched with calculated frequencies using a wavenumber range of ±24 cm^{-1}. In cases where corresponding peaks are assigned with a large variation in wavenumber (e.g., 24 cm^{-1}), the lack of goodness of fit will be reflected in the linear regression analysis. For the model glutamate deprotonated at both carboxyl groups, the calculated frequencies do not predict a peak at 1593 cm^{-1}, leading to the one instance where an observed peak is not matched by a calculated peak. This IR peak is predicted at pH 3 (1596 cm^{-1}), and it is possible that some glutamates are not deprotonated at both carboxyl groups up to pH 7.1, leading to the presence of this peak at both pH 3 and 6 in the observed spectra and its absence in the model.

The spectra for aspartate are generally similar to those for glutamate, and the band assignments at pH 3 and 6 are given in Table 3. Differences between the carboxyl groups are harder to detect; however, the peak at ∼1600 cm^{-1} can be assigned to ν_{as}(α-COO$^-$) and changes to this peak upon reaction can be attributed to interaction with the α-carboxyl. Decreasing the pH of aspartate results in protonation of the γ-carboxyl, increasing the wavenumber ratio of ∼1420:1395, and a peak corresponding to ν(γ-C═O) appears around 1720 cm^{-1}.

3.2. FTIR Spectra of Glutamate Interactions with Rutile Films. IR spectra of glutamate at 4.4, 1.0, and 0.1 mmol kg^{-1} at pH 3.3 and 5.8 are shown in Figure 5 along with a reference spectrum of aqueous glutamate (40 mmol kg^{-1}). Peak locations

(29) Becke, A. D. *J. Chem. Phys.* **1997**, *107*, 8554–8560.
(30) Lee, C. T.; Yang, W. T.; Parr, R. G. *Phys. Rev. B* **1988**, *37*, 785–789.
(31) Rassolov, V. A.; Ratner, M. A.; Pople, J. A.; Redfern, P. C.; Curtiss, L. A. *J. Comput. Chem.* **2001**, *22*, 976–984.
(32) Wong, M. W. *Chem. Phys. Lett.* **1996**, *256*, 391–399.
(33) Yamaguchi, Y.; Frisch, M.; Gaw, J.; Schaefer, H. F.; Binkley, J. S. *J. Chem. Phys.* **1986**, *84*, 2262–2278.
(34) Frisch, M. J.; Yamaguchi, Y.; Gaw, J. F.; Schaefer, H. F.; Binkley, J. S. *J. Chem. Phys.* **1986**, *84*, 531–532.
(35) Schaftenaar, G.; Noordik, J. H. *J. Comput.-Aided Mol. Des.* **2000**, *14*, 123–134.
(36) Fitts, J. P.; Persson, P.; Brown, G. E.; Parks, G. A. *J. Colloid Interface Sci.* **1999**, *220*, 133–147.
(37) Pearson, J. F.; Slifkin, M. A. *Spectrochim. Acta, Part A* **1972**, *A 28*, 2403–&.
(38) Imamura, K.; Mimura, T.; Okamoto, M.; Sakiyama, T.; Nakanishi, K. *J. Colloid Interface Sci.* **2000**, *229*, 237–246.

Table 1. Important FTIR Band Assignments for Aqueous Glutamate Based on Previously Published Studies[1,36,37] and Calculated in This Work[a]

experimental			calculated			
glutamate peaks[b]	pH 3	pH 6	glutamate peaks (pH 3)[c]	pH 3	glutamate peaks (pH 6)[c]	pH 6
ν(γ-C═O)	1723		δ(HNH)	1732		
$\nu_{as}(NH_3^+)$	1625 (w)	1625 (w)	ν_{as}(α-COO^-)	1621, 1657 (w)		
ν_{as}(α-COO^-)	1598	1593	ν_{as}(γ-COOH)	1596	ν_{as}(α-COO^-)	1619
ν_{as}(γ-COO^-)		1562	δ(HNH)	1568	ν_{as}(γ-COO^-)	1541
ν_{as}(γ-COO^-), $\nu_s(NH_3^+)$	1527		$\nu_s(NH_3^+)$, δ(COH)	1534		
$\delta(CH_2)$	1450	1450	$\delta(CH_2)$, $\omega(CH_2)$	1378, 1382, 1421, 1472(w)	$\delta(CH_2)$	1442 (w)
ν_s(α-COO^-), ν_s(γ −COO^-)	1405	1402	ν_s(α-COO^-)	1339	ν_s(γ-COO^-)	1391
$\omega(CH_2)$	1350	1348	backbone	1348	backbone	1353
ν(CO), δ(OH)	1227		δ(γ-COOH)	1248	$\rho(CH_2)$	1223

[a] Vibrational mode: ν = stretching, δ = bending, ω = wagging, ρ = rocking; w = weak relative peak strength. [b] Peak assignments from previously published studies.[1,36,37] [c] Peak assignments calculated in the current work.

Table 2. Linear Regression Analysis of Experimental FTIR Peak Wavenumber Data Versus Calculated Results for Aqueous Glutamate[a]

model	glutamate sample	N	intercept (std error)	slope (std error)	R^2 (std error)[b]
pH 3 glutamate-aqueous	pH 3: 40 mM (aq)	8	11.0 (50.0)	0.99 (0.33)	0.993 (14.3)
pH 6 glutamate-aqueous	pH 6: 40 mM (aq)	5[c]	59.6 (59.5)	0.96 (0.04)	0.995 (9.17)

[a] N represents the number of observed experimental peaks matched (via wavenumber) with a corresponding calculated peak, and RMSE is the root mean square error. [b] R^2 standard error is the RMSE. [c] One unmatched FTIR peak at 1593 cm^{-1}.

Table 3. Important FTIR Band Assignments for Aqueous Aspartate Based on Previously Published Studies[2,37]

	experimental	
aspartate peaks	pH 3	pH 6
ν(γ-C═O)	1719	
ν_{as}(α-COO^-)	1602	1598
$\nu_s(NH_3^+)$	1510	1485,1468
ν_s(α-COO^-), $\delta(CH_2)$	1418	1421
ν_s(α-COO^-), ν_s(γ −COO^-)	1394	1392
$\omega(CH_2)$	1356	1355
$\delta(CH_2)$	1305	1307

and assignments are given in Table 4, and peak intensities are given in the Supporting Information (Tables S2 and S3). The spectra for 4.4 and 1.0 mmol kg^{-1} are very similar having small differences from the 0.1 mmol kg^{-1} spectrum for both pH values examined. Comparing the glutamate aqueous spectra with 4.4 and 1.0 mmol kg^{-1} after reaction with rutile at pH 3, the most notable difference is the lack of a peak within 1715−1735 cm^{-1}, commonly assigned to carbonyl vibrations.[1,36,37] The pH dependency of this peak can be observed through examination of FTIR glutamate spectra collected as a function of solution pH (Figure 3). Since pH 3 is below the pK_a for the γ-carboxyl group, a peak around 1720 cm^{-1} (C═O) is expected unless the carboxyl group is involved in binding to the rutile surface. Therefore, it is hypothesized that binding of glutamate to rutile occurs at least, in part, through the γ-carboxyl group. A similar study examining the binding of glutamate to alumina also attributed interaction between γ-carboxyl group and the surface to inhibition of carboxylate protonation at pH 4.5 due to the lack of a corresponding C═O IR band.[36] For 0.1 mmol kg^{-1} glutamate samples, the presence of small IR bands at 1730 and 1745 cm^{-1} for pH 3 and 6, respectively, represents C═O from either α- or γ-carboxyl groups. At pH 3, aqueous glutamate results in a C═O peak at 1716 cm^{-1}, and at pH 6 no C═O is present as both carboxyl groups are deprotonated. Although contributions to IR bands corresponding to C═O of the α-carboxyl are not observed above pK_{a1} (pH = 2.2) for aqueous glutamate, the bands at 1730 and 1745 cm^{-1} for glutamate bound to rutile cannot be unequivocally assigned to γ-carboxyl, as adsorption can affect the acidity of the carboxyl groups; covalent bonding alters the electronic structure of the molecule and may lead to protonation of the α-COOH above its aqueous phase pK_a value.[19,39] Additionally, the dielectric constant of water near the surface of a mineral is much lower than the bulk dielectric constant of water.[40] Since lower dielectric constants favor less charged molecules, the presence of α-COOH is possible if glutamate binds to rutile via γ-carboxyl.

Other notable differences in spectra include a reduction in the intensity of 1405 [$\nu_s(COO^-)$] and 1523 cm^{-1} [ν_{as}(γ-COO^-), $\nu_s(NH_3^+)$] relative peak intensity, along with a shift in the 1596 cm^{-1} [ν_{as}(α-COO^-)] to ∼1620 cm^{-1}. The decreased contribution in carboxyl peaks around 1400 cm^{-1} to the spectra is attributed to their complexation with the rutile surface and the presence of new peaks corresponding to ν_{as}(γ-COO^-), ν_{as}(α-COO^-), and ν_{as}(γ-C═O) at 1560, 1620, and 1640 cm^{-1}, respectively. The low glutamate concentration spectrum (0.1 mmol kg^{-1}) has a peak at 1638 cm^{-1} which is attributed to ν(γ-C═O), and the 1400 cm^{-1} peak [ν_s(α-COO^-), ν_s(γ-COO^-)] is no longer present; however, a small peak at 1425 cm^{-1} [ν_s(γ-COO^-)] is observed. It should be noted that band assignments from 1620 to 1640 cm^{-1} can be compromised due to incomplete subtraction of water and therefore some reduction in confidence of assignment exists for these wavenumbers. However, the fact that this peaks shift for different amino acid concentrations is observed (water absorption is fixed at ∼1630 cm^{-1}), and that this peak is not present for water subtractions with aspartate (Figure 7), suggests that subtraction errors are minimal. The difference in spectra for high and low glutamate concentrations reacted with rutile films suggests that more than one binding mechanism, or surface species, is present. In particular, multiple binding mechanisms are likely for high concentration experiments where monolayer coverage may be exceeded. Overall, the FTIR results strongly suggest that sorption of glutamate to rutile occurs through covalent bonding via the γ-carboxyl. Determination of the role of the α-carboxyl and specific binding mechanism (e.g., monodentate, bidentate) is not possible via FTIR data alone, and correlation of data with quantum chemical calculations is used to elucidate surface species.

(39) Duckworth, O. W.; Martin, S. T. *Geochim. Cosmochim. Acta* **2001**, *65*, 4289–4301.
(40) Teschke, O.; Ceotto, G.; de Souza, E. F. *Phys. Rev. E* **2001**, 64.

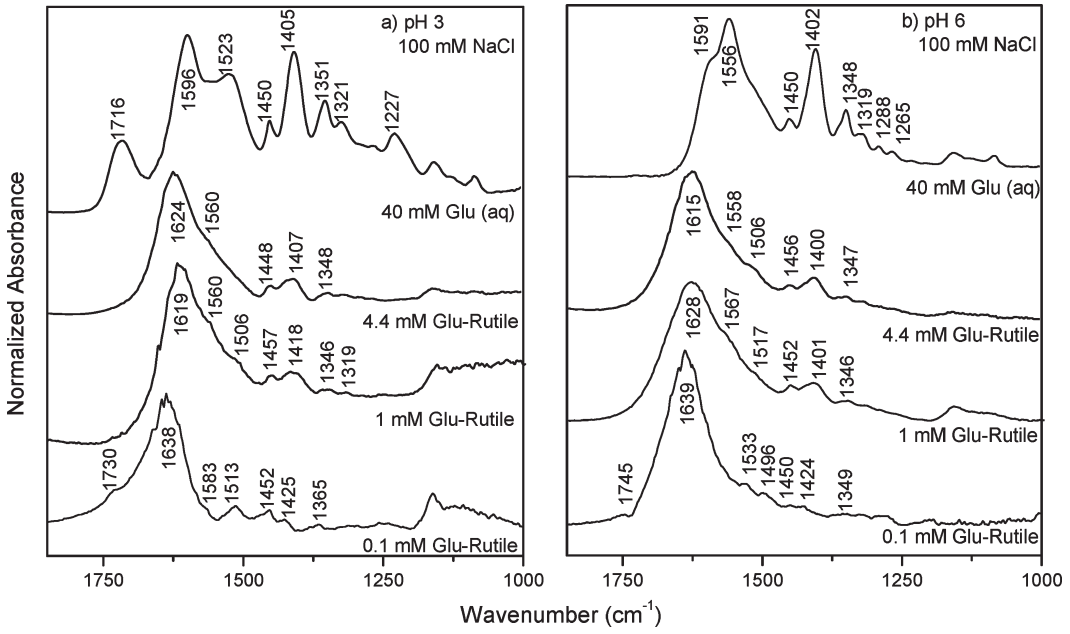

Figure 5. ATR-FTIR spectra of glutamate (Glu) adsorbed to rutile films at (a) pH 3 and (b) pH 6 (mM = mmol kg^{-1}).

Table 4. FTIR Peak Locations (cm^{-1}) for Glutamate Reacted with Rutile Films Based on Peak Assignments in Table *1* and Quantum Chemical Calculations (Current Study)[a]

	pH 3			pH 6		
glutamate peaks	4.4 mmol kg^{-1}	1.0 mmol kg^{-1}	0.1 mmol kg^{-1}	4.4 mmol kg^{-1}	1.0 mmol kg^{-1}	0.1 mmol kg^{-1}
$\nu(\gamma\text{-C=O})$			1730			1745
$\nu_{as}(\alpha\text{-COO}^-)$	1624	1619	1614(sh)	1615	1628	1621(sh)
$\nu(\alpha\text{-C=O})$			1638			1639
$\nu_{as}(\gamma\text{-COO}^-)$	1560	1506, 1560	1513, 1583	1506, 1558	1567	1496, 1533
$\delta(CH_2)$	1419, 1448	1418, 1457	1425, 1452	1456	1452	1424, 1450
$\nu_s(\alpha\text{-COO}^-)$, $\nu_s(\gamma\text{-COO}^-)$	1410	1404	1365 (w)	1400	1401	1349 (w)
$\omega(CH_2)$	1348	1346		1347	1346	

[a] sh = peak located in a shoulder position; *w* = weak relative peak strength.

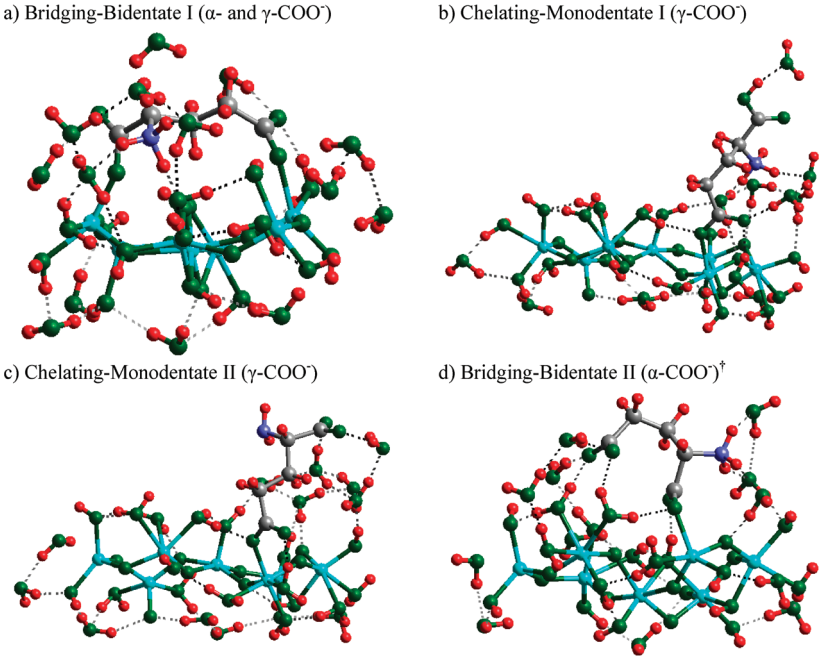

Figure 6. Surface speciation models resulting from quantum chemical calculations for aqueous glutamate reacted with the (101) surface of rutile; (†) outer-sphere coordination through $\gamma\text{-COO}^-$ also present. In all surface species, H-bonding (dashed lines) between carboxyl groups attached to the rutile surface is present for O atoms not covalently bound.

Table 5. Frequency (cm^{-1}) of Carboxyl Group Interactions with the (101) Surface of Rutile via Quantum Chemical Calculations for the Four Models Which Most Closely Match Experimental Data

	bridging-bidentate I (α- and γ-COO^-)	chelating-monodentate I (γ-COO^-)	chelating-monodentate II (γ-COO^-)	bridging-bidentate II (α-COO^-)[a]
ν(α-C═O)	1632	1728		1676
ν(γ-C═O)	1579			
ν_{as}(α-COO^-)			1615	
ν_{as}(γ-COO^-)		1601	1593	1565
ν_s(α-COO^-)	1366		1325	1246
ν_s(γ-COO^-)	1366	1390	1349, 1361	1401, 1361
ν_s(α-COH)		1373, 1470		

[a] Outer-sphere coordination through γ-COO^- also present.

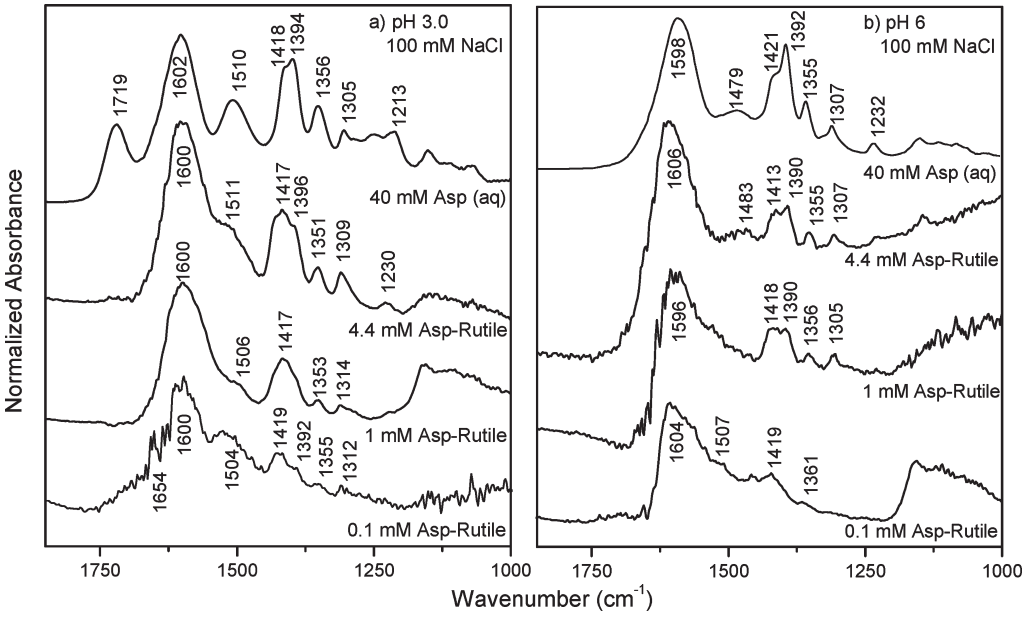

Figure 7. ATR spectra of aspartate (Asp) adsorbed to rutile films at (a) pH 3 and (b) pH 6 (mM = mmol kg^{-1}).

3.3. Surface Speciation Models of Glutamate Interactions with Rutile Films. Review of the 13 potential surface configurations of glutamate on the (101) surface of rutile as determined via quantum chemical calculations revealed four models which predict IR peak locations similar to experimental data (Tables 4 and 5, Figure 6). The wavenumber values of IR bands corresponding to carboxyl groups in calculated and experimental data were used as a primary method for comparison (Tables 4 and 5). All predicted surface species models indicate glutamate carboxyl groups bind to rutile through a combination of inner-sphere, outer-sphere, and direct H-bonding. In all surface species, H-bonding between carboxyl groups attached to the rutile surface is present for O atoms not covalently bound to the surface. In Figure 6a (bridging-bidentate I; BBI), glutamate is "lying down" and binding occurs through both the α- and γ-carboxyl groups; in total, there are four points of attachment with one inner-sphere bond (Ti−O−C) and one H-bond (Ti−OH_2^+···O═C) for each carboxyl group. Figure 6b and c (chelating monodentate; CMI and CMII) represent glutamate binding through the γ-carboxyl group in a "standing up" configuration. In these models, there is one covalent bond (Ti−O−C) and one H-bond (Ti−OH_2^+···$^-$O−C) for the γ-carboxyl, leading to two points of attachment to the rutile surface. These chelating-monodentate models are quite similar, with binding occurring via the γ-carboxyl group; the difference being protonation of the α-carboxyl in Figure 6b (CMI). For Figure 6d (bridging-bidentate II; BBII), glutamate is binding to rutile via the α-carboxyl group, and outer-sphere coordination between the γ-carboxyl group and rutile results in the molecule "lying down". In this model, there are a total of four points of attachment, with one inner-sphere covalent bond (Ti−O−C) and one H-bond (Ti−OH···O═C) for the α-carboxyl group, and two outer-sphere bonds (Ti−OH_2^+···OH_2···$^-$O−C) for the γ-carboxyl group.

Linear regression analysis of experimental FTIR data versus predicted peak location from quantum chemical calculations (e.g., Kubicki et al.[9]) was also conducted to determine which models best match the observed results (Table 6). Since differences between high and low glutamate concentrations suggest more than one surface species with increased concentration, focus is given to the 0.1 mmol kg^{-1} glutamate experiments where a single surface configuration is more likely, and regression data for higher glutamate concentrations are provided in the Supporting Information (Table S1). To determine which models provide the best match to the experimental data, the *y*-intercept, slope, and correlation coefficient (R^2) are considered. The four models considered all fit the observed IR peak locations well, and only slight differences in correlation parameters are present. For the 0.1 mmol kg^{-1} data, it is possible to exclude BBI (Figure 6a), CMI (Figure 6b), and CMII (Figure 6c) for pH 3 and BBI (Figure 6a) and CMI (Figure 6b) for pH 6 based on values of *y*-intercept, slope, standard error, and R^2. Of the remaining models, the pH 3 data is best represented by CMI and BBII (Figure 6b, d) and the pH 6 data is best represented by BBII (Figure 6d). Calculated

Table 6. Linear Regression Analysis of Experimental FTIR Data (0.1 mmol kg^{-1} Glutamate; pH 3 and 6) versus Calculated Results (Regression Data for 1 and 4.4 mmol kg^{-1} Glutamate Are Given in the Supporting Information)[a]

model	glutamate sample	N	y-intercept (std error)	slope (std error)	R^2 (std error)[b]
bridging-bidentate I (α- and γ-COO^-)[c]	pH 3	7	89.7 (96.7)	0.93 (0.06)	0.973 (19.9)
bridging-bidentate I (α- and γ-COO^-)[d]	pH 6	7	172 (145)	0.88 (0.99)	0.934 (31.4)
chelating-monodentate I (γ-COO^-)[e]	pH 3	7	−21.5 (118)	1.02 (0.07)	0.966 (24.5)
chelating-monodentate I (γ-COO^-)[c]	pH 6	7	206 (99.7)	0.86 (0.07)	0.967 (21.6)
chelating-monodentate II (γ-COO^-)[c]	pH 3	6	−199.36 (176)	1.12 (0.12)	0.947 (27.1)
chelating-monodentate II (γ-COO^-)	pH 6	7	−375.5 (147)	0.73 (0.10)	0.904 (31.8)
bridging-bidentate II (α-COO^-)[e]	pH 3	7	−2.73 (127)	1.00 (0.08)	0.960 (26.3)
bridging-bidentate II (α-COO^-)[c]	pH 6	7	51.0 (114)	0.96 (0.07)	0.965 (24.7)

[a] N represents the number of observed experimental peaks matched (via wavenumber) with a corresponding calculated peak. [b] R^2 standard error is the RMSE. [c] Poorest fits between experimental and calculated results based on comparison of all four parameters: slope, y-intercept, R^2, and RMSE. [d] Best fits at pH 6. [e] Best fits at pH 3.

Table 7. Corresponding Calculated and Experimental Frequencies for Carboxyl Groups (Glutamate Bound to Rutile) Used for Correlating between Modeled and Experimental Data[a]

calculated frequency (cm^{-1})			experimental frequency (cm^{-1})	
bridging-bidentate I	bridging-bidentate II	chelating-monodentate I	pH 3	pH 6
1721[b]	1676	1728[c]	1730[c]	
1632[c]	1636[b,c]	1601	1638[c]	1639[c]
1579[c]	1565[c]	1553[b,d]	1583[c]	1533[d]
		1470[c]	1452[c]	1450[c]
	1401[c]	1390	1425[c]	1424[c]
1366[c]	1361[c]	1373[c]	1365[c]	1349
	1246			

[a] Carboxyl group band assignments for calculated frequencies are given in Table 5. [b] Designates calculated frequencies which, based on calculations, do not correspond to carboxyl groups but are included in the table because frequency values are close to experimental and other model calculations corresponding to carboxyl groups. [c] Frequencies which have been determined to match between experimental and calculated results. [d] Frequencies which have been determined to match between experimental and calculated results for rows with more than one set of matching frequencies.

peak intensities corresponding to synthetic spectra for these three surface species are given in the Supporting Information (Figure S1).

Corresponding frequenices for experimental and calculated results attributed to carboxyl groups of glutmate bound to rutile (from modeling results) are shown in Table 7. Although a high degree of correlation exists, as well as numerous matched frequencies, between experimental and calculated data, there are instances where calculated peaks are not reproduced in the experimental data (Supporting Information Figure S1). In these instances, some of the peaks present in the calculated spectra may not be observed in experimental data for three primary reasons. The first is that some bands might be below experimental IR detection limits. By comparing spectra for 40 mmol kg^{-1} glutamate with spectra at lower concentrations, it is apparent that fewer peaks are observed at lower concentrations (Figure 5). Many of the experimental frequencies that are unmatched by the 0.1 mmol kg^{-1} Glu bound to rutile do match with peaks present in the 40 mmol kg^{-1} Glu (e.g., 1081, 1227, 1321, 1591, 1596 cm^{-1}). Second, even if water subtraction from IR spectra is done with perfect accuracy, the potential for bound water to remain still exists. The peaks for bound water will occur at frequencies which differ slightly from aqueous O−H vibrations and therefore may not be completely removed with spectral subtractions. This may help to explain the large peaks present 1600−1700 cm^{-1} which potentially mask other vibrational modes which are observed in the calculated spectra. And third, although a high degree of confidence exists in the water subtractions, any errors in the subtraction can lead to unwanted peaks which again can mask frequencies observed through calculations.

The proposed structures of the surface species are in overall agreement with those predicted using the extended triple-layer model (ETLM) via the GEOSURF computer code.[6] In that study, the ETLM predicted two surface complexes with an alternative for each: Figure 6a (BBI) or d (BBII; with H-bonding through the γ-carboxyl, but without water bridging), and "standing up" species such as Figure 6c (CMII; with no C═O on the γ-carboxyl) or an outer-sphere equivalent bound through the γ-carboxyl via H-bonding (not predicted in the current study). However, the surface complexation modeling predicted that the "standing up" species is predominant at pH = 6 and a "lying down" species at pH = 3, whereas the reverse is suggested in the current study at pH 6 (BBII) and either "standing up" (CMI) or "lying down" (BBII) at pH 3, based on the slight difference in fit between the theoretically calculated and the measured IR frequencies (Table 6). The overall agreement in the structures of the surface species between the surface complexation modeling and the present study provides additional validity to the observed/predicted results. Similar configurations were also predicted for glutamate binding to amorphous TiO_2[7] based on interpretation of published ATR-FTIR data.[1]

3.4. FTIR Spectra of Aspartate Interactions with Rutile Films. FTIR spectra of aspartate bound to rutile do not change significantly with variation in pH or aspartate concentration (Figure 7, Table 8) and suggest the presence of outer-sphere surface species. Compared to aqueous phase aspartate at pH 3, the ν(γ-C═O) peak at 1720 cm^{-1} is not present and there is a reduction in $\nu_s(NH_3^+)$ (1510 cm^{-1}) peak intensity upon reaction with rutile. The 0.1 mmol kg^{-1} (pH 3 and 6) spectra do show a slight shift in the ν_{as}(α-COO^-) band (1600 cm^{-1}). Spectra for 4.4 and 1.0 mmol kg^{-1} aspartate (pH 6) reacted with rutile appear to have no distinct differences from aqueous aspartate. At pH 6, sorption of 1 mmol kg^{-1} aspartate is slightly less than 1 mmol kg^{-1} glutamate to rutile (aspartate, 0.45 μmol m^{-2}; glutamate, 0.60 μmol m^{-2}),[5,6] and therefore, reacted spectra may be somewhat

Table 8. FTIR Peak Locations for Aspartate Reacted with Rutile Films Based on Peak Assignments in Table 2,[a]

	pH 3			pH 6		
aspartate peaks	4.4 mmol kg^{-1}	1.0 mmol kg^{-1}	0.1 mmol kg^{-1}	4.4 mmol kg^{-1}	1.0 mmol kg^{-1}	0.1 mmol kg^{-1}
ν_{as}(α-COO^-)	1600	1600	1600	1606	1596	1604
$\nu_s(NH_3^+)$	1511	1506	1504	1483	1515	1507
$\delta(CH_2)$, ν_s(α-COO^-)	1417	1417	1419	1413	1418	1419
ν_s(α-COO^-), ν_s(γ−COO^-)	1396	1396	1392	1390	1390	1395 (w)
$\omega(CH_2)$	1351	1353	1355	1355	1356	1361
$\delta(CH_2)$	1309	1314	1312	1307	1305	

[a] w = weak relative peak strength.

more difficult to resolve. Although some spectra have an undesirable signal-to-noise ratio in the region where water and water vapor strongly absorb (~1750−1550 cm^{-1}), spectral quality is adequate and analysis of spectra can be conducted. In general, the spectra of aspartate reacted with rutile resemble the aqueous phase spectra of aspartate at pH 6 over the concentration range and pH values examined. The disappearance of the ν(α-C═O) peak (1720 cm^{-1}) at pH 3 suggests binding of aspartate through the α-carboxyl group. In the spectra of aspartate adsorbed to rutile, there are no new peaks or peak shifts (compared to aqueous phase aspartate), but a relative decrease in ν_s(α-COO^-) and ν_s(γ-COO^-) around 1400 cm^{-1} compared to other peaks (e.g., ~1600 cm^{-1}) is observed. Changes in the contributions of IR absorbing groups to the spectra indicate some interaction with the surface, likely resulting from weak binding mechanisms such as formation of outer-sphere complexes. If binding occurred via inner-sphere coordination, it is expected that COO^- peaks would shift and/or disappear.[1,41−43] From the current data, the specific configuration, or number of possible configurations, cannot be absolutely ascertained, and it is predicted that relatively weak outer-sphere sorption via a "lying down" conformation would not alter the molecular structure significantly from the solution phase and thus spectra resemble aqueous aspartate at pH 6. This result is consistent with previous ATR-FTIR studies examining the binding of aspartate to amorphous TiO_2.[1] It should be noted that surface complexation modeling of aspartate adsorption on rutile suggested two surface complexes, one "lying down" and one "standing up".[5] The stoichiometry of the reactions for the formation of these two complexes can both be interpreted as forming outer-sphere surface complexes. Combining this inference with the results of the present study suggests that both hypothesized surface species are outer-sphere complexes.

Sum frequency generation vibrational spectroscopy has previously been used to study the binding of aspartate and glutamate to an unspecified hydrophilic TiO_2, indicating that both carboxylic groups are involved in binding to the mineral surface.[2] In that study, one of the carboxyl groups coordinates with the surface via a monodentate bond while the other binds through H-bonding, analogous to Figure 6d (for glutamate). Data supporting monodentate binding through aspartate carboxyl group was not observed in this current study; however, binding through both carboxyl groups in a "lying down" configuration is consistent. It has also been previously suggested that the sorption of aspartate to TiO_2 surfaces can occur via amino functional groups.[44] Our results do not suggest interaction between basic amino groups and the rutile surface. The results in this study, both experimental and calculated, provide strong evidence for glutamate and aspartate interacting with rutile only via their carboxyl groups (inner-sphere and/or outer-sphere coordination), which is in agreement with the majority of studies exploring their interactions with metal oxide surfaces.[2,5−8,36]

4. Conclusions

The data presented in this paper enhances current interpretations of glutamate binding mechanisms to rutile surfaces and highlights the importance of both covalent and H-bonding mechanisms. The data indicate that pH (3 vs 6) has a slight effect on glutamate sorption to rutile and may lead to subtle differences in surface species present. While binding of aspartate is believed to occur though a "lying down" outer-sphere coordination (pH 3 and 6), multiple inner-sphere complexes of glutamate ("lying down" or "standing up") that are influenced by solution pH are hypothesized. The evaluation of ATR-FTIR data and quantum chemical calculations reveals a minimum of at least one covalent bond between glutamate carboxyl groups and rutile. Comparison of results from modeling ATR-FTIR spectra were limited to the experimental low concentrations (0.1 mmol kg^{-1} glutamate), where the probability of exceeding monolayer coverage is reduced. Calculated IR peak wavenumbers were in very good agreement with experimental data and suggest three main surface species. The species include a bidentate-bridging species, where inner-sphere coordination between one O atom of each carboxyl group to the rutile surface is observed along with H-bonding of the other two carboxyl O atoms. Also hypothesized are species where one covalent bond is formed between either the α- or γ-carboxyl group and that the molecule maybe be "standing up" and anchored through monodentate coordination of the γ-carboxyl, or "lying down" with inner-sphere binding of the α-carboxyl and outer-sphere coordination of the γ-carboxyl group. This paper presents novel data, using ATR-FTIR spectroscopy and advanced modeling techniques, which are in general agreement with previous interpretations of surface complexation models of glutamate and aspartate sorption to rutile, while providing additional clarity to subtle nuances of specific binding mechanisms.

Acknowledgment. The authors are grateful for the rutile sample provided by J. Rosenqvist and D. Wesolowski of the Oak Ridge National Laboratory, as well as M. Machesky of the Illinois State Water Survey. The authors thank Mengqiang Zhu for helpful discussions early on and for initiating the quantum chemical modeling for this research. This publication was made possible, in part, by the National Science Foundation EPSCoR Grant No. EPS-0814251 and the State of Delaware. Additional support for C.M.J., C.L.J., D.A.S., and R.M.H. was provided by a NSF-NASA Collaborative Research Grant to the Johns Hopkins University and the Carnegie Institution for Science. D.A.S. also

(41) Tejedor-Tejedor, M. I.; Yost, E. C.; Anderson, M. A. *Langmuir* **1990**, *6*, 979–987.
(42) Persson, P.; Karlsson, M.; Ohman, L. O. *Geochim. Cosmochim. Acta* **1998**, *62*, 3657–3668.
(43) Borer, P.; Hug, S. J.; Sulzberger, B.; Kraemer, S. M.; Kretzschmar, R. *Geochim. Cosmochim. Acta* **2009**, *73*, 4661–4672.
(44) Giacomelli, C. E.; Avena, M. J.; Depauli, C. P. *Langmuir* **1995**, *11*, 3483–3490.

acknowledges support from DOE Grant DE-FG02-96ER-14616. Computations were supported by the Materials Simulation Center, a Penn State MRSEC and MRI facility.

Supporting Information Available: Table showing complete regression results for experimental FTIR data versus calculated results (Table S1); tables giving IR absorbance values from glutamate and aspartate adsorption experiments (Tables S2−S4); figure showing the synthetic IR spectra (Figure S1) for the most probable surface species. This material is available free of charge via the Internet at http://pubs.acs.org.